# INVESTIGATION OF $CO_2$ DILUTED METHANE AND PROPANE SWIRLING PREMIXED FLAMES USING $CH^*$ CHEMILUMINESCENCE IMAGING

by

***Vuk M. ADŽIĆ[a], Aleksandar M. MILIVOJEVIĆ[a*], Mirjana S. STAMENIĆ[a], and Miroljub M. ADŽIĆ[a,b]***

[a] Faculty of Mechanical Engineering, University of Belgrade, Beograd, Serbia
[b] Academy of Engineering Sciences of Serbia, (AESS), Belgrade, Serbia

Original scientific paper
https://doi.org/10.2298/TSCI180312375A

*Utilization of hydrocarbon gaseous fuels, such as biogas, landfill gas and others, is a valuable contribution to sustainable energy production and climate changing control. The presence of $CO_2$ in these gases decreases heat of combustion, flame temperature, flame speed and can induce flame blow-off and combustion instabilities. In order to better understand the problem, flame geometry and location was investigated using chemiluminescence ($CH^*$) imaging technique. Combustion took place in a purposely built, lean, premixed, unconfined swirl burner, fueled by methane and propane diluted with $CO_2$. The fuel type, air-to-fuel equivalence ratio and $CO_2$ content were chosen as the independent variables. The $CH^*$ imaging by means of a commercial CCD camera, fitted with an optical filter, was used for flame investigation. The analysis of images showed that the $CH^*$ emission intensity, flame geometry and location were remarkably affected by the fuel type and the air-to-fuel equivalence ratio, while the $CO_2$ dilution was of minor importance.*

Key words: *methane-propane combustion, $CO_2$ addition, commercial CCD camera, swirling premixed unconfined flame, chemiluminescence imaging*

## Introduction

The Paris climate accord of 2015 aims to support the global action to control the climate change by keeping a global temperature rise in this century below 2 degrees above the pre-industrial levels [1]. The proposed action mechanism is to strengthen the mitigation of GHG and to support sustainable development, which includes RES and actions to improving energy efficiency. Utilization of biomass, such as biogas and landfill gases, is an important contribution to such efforts. Biogases are mixtures of $CH_4$ (45-70% by volume) and ballast components, mainly $CO_2$ (30-60%), and to far less extent, nitrogen (0-5%). The presence of ballast components in combustible gases decreases their calorific value, flame temperature, laminar flame speed, narrows flammability limits, affects emissions and increases susceptibility of flame to blow-off and instabilities [2-4]

While the adiabatic flame temperature and laminar flame speed are inherent characteristics of a fuel-oxidizer mixture composition, the flame blow-off and flame instabilities are controllable to a certain extent. The principle of flame stabilization is based on enabling chemical reactions to finish in a given space over a range of operating conditions. There are a number of methods to stabilize a flame, of which most often used are bluff body, swirl, dump and piloted

* Corresponding author, e-mail: amilivojevic@mas.bg.ac.rs

flame methods. This investigation applies swirl method for flame stabilization. A swirl is the most effective aerodynamic method of flame stabilization.

The present paper deals with a premixed flame using swirl to stabilize the flame. The more detailed explanation of the aerodynamic techniques for flame stabilization can be found elsewhere [5-10]. In short, the bluff body flow is characterized by a recirculation zone behind the body with and shear flow, outer region. The flow produces a turbulent exchange of heat and mass which heats-up the incoming fuel-air mixture, mixes it with the combustion products, and increases the residence time for the chemical reactions. The similar flow pattern stands for dump flows, as well. A swirl is relatively simple yet the most effective aerodynamic method for flame stabilization [5-10]. A swirling flow, schematically shown in fig. 1, induces a complex recirculation zone which entrains outer hot combustion products and mixes them with the incoming fuel and air mixture. It is characterized by strong turbulence field and mixing on both micro and macro levels. Strong turbulence increases a turbulent flame velocity, which further increases flame stability. In addition, due to its excellent flame stabilization characteristics, swirl enables combustion of very lean mixtures which is favorable for very low emission of $NO_x$ [11-13].

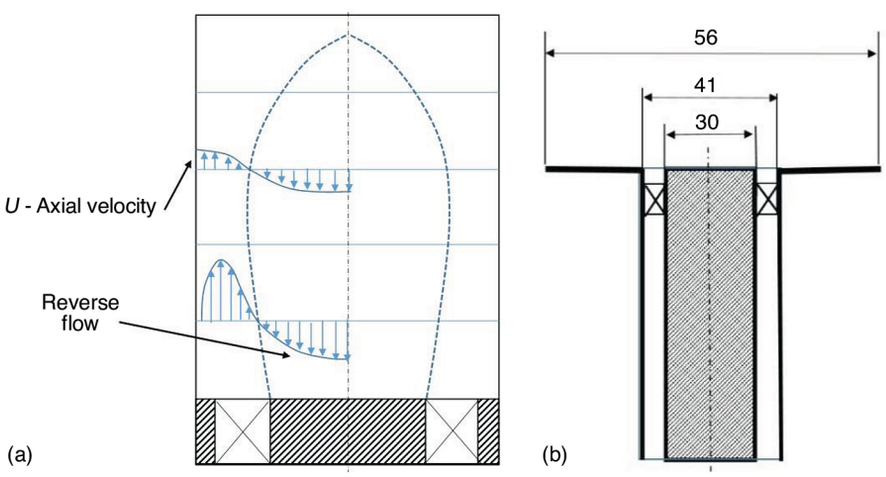


**Figure 1. Schematics of swirling flow (a) and swirl burner (b) [mm]**

The complex nature of turbulent, swirl flame is still not fully understood. Flame visualization techniques have been used for decades to investigate flames. They are non-intrusive methods that can give instantaneous information on flame geometry, location and flame behavior [14, 15]. Development of CCD cameras and computerized image processing has further fostered interest in the application of visualization techniques for combustion research. Flame chemiluminescence [5, 16] is a valuable and proved imaging technique for flame research. It can provide important information, such as flame geometry, location of zones of maximum heat release rate, air to fuel equivalence ratio, $\lambda$, adiabatic flame temperature, flame instabilities and others [5-10, 17, 18].

Jensen [5] presented state of the art of general techniques and instruments used for luminescence visualization, measurements and analysis. Bheemul *et al*. [6] used a set of CCD cameras to capture 2-D images of flame. A numerical algorithm was developed to present the grabbed images into 3-D ones. The authors showed that the system was capable to present the flame geometric parameters for different combustion conditions. The chemiluminescence emissions of $OH^*$, $CH^*$, $C_2^*$, and $CO_2^*$ in natural gas/air premixed counter flow flames, with

variable equivalence ratio, were measured by a high performance spectroscopic unit [7]. The obtained results showed that chemiluminescence intensities of $OH^*$, $CH^*$, and $CO_2^*$ were suitable indicators for heat release rates and equivalence ratios. Guethe *et al*. [8] overviewed possible application of chemiluminescence for gas turbine combustor development including correlation between the heat release rate and $NO_x$ formation processes. They found that flame chemiluminescence imaging was useful technique for combustor research and development regarding flame stability and emissions. The effect of propane ($C_3H_8$), isooctane, ethanol, and methanol on equivalence ratio measurements using chemiluminescence was investigated by Orain and Hardalupas [9]. The authors concluded that the $OH^*/CH^*$ intensities ratio had monotonic relation with equivalence ratio for all test fuels, except for ethanol and methanol flames, when the effect of flame strain rate had to be considered. The chemiluminescence emissions of $OH^*$, $CH^*$, $C_2^*$, and $CO_2^*$ were analyzed as a function of equivalence ratios in atmospheric $CH_4$-air premixed flames [10]. The same authors developed a multivariate sensing methodology to match the experimentally measured equivalence ratios in premixed $CH_4$-air flames. The $OH^*/CH^*$ intensities ratio was used as a marker for prediction of equivalence ratios. Simona *et al*. [17] used the chemiluminescence 309 and 282 nm bands to investigate the effect of butanol-diesel fuel blends on spray combustion in a common rail Diesel engine. The ratio of the intensities was used to follow the flame temperature evolution. Jozsa and Sztanko [18] used flame $OH^*$, $CH^*$, and $C_2^*$ emission spectroscopy to compare the steam-blast atomization and the air-blast atomization of a diesel oil in an atmospheric, lean, prevaporized, premixed burner. The ratios of $OH^*/CH^*$, $OH^*/C_2^*$, and $CH^*/C_2^*$ chemiluminescence intensities were used as markers. The authors concluded that the steam blast atomization resulted in lower adiabatic flame temperature compared to the air blast atomization. The temperature reduction lowered the $C_2^*$ luminescence intensity more than the intensities of $OH^*$ and $CH^*$.

While many investigations deal with $CH_4$, $C_3H_8$, isooctane, methanol, ethanol, butanol, diesel, kerosene and other fuels [5-10, 17, 18], few were concerned with biogas, or $CH_4$ and $CO_2$ blends [19-25]. Guiberti *et al.* [19] used combined numerical and experimental investigation of $OH^*$, $CH^*$, and $CO_2^*$ chemiluminescence intensities of a laminar, premixed, conical $CH_4$ flames, as a function of dilution with $CO_2$ and $N_2$ using a spectrometer and an ICCD camera fitted with optical filters. Marsh *et al*. [20] used a CCD camera coupled with an optical filter for $OH^*$ chemiluminescence in $CH_4$-air premixed confined swirl flames, diluted with $CO_2$ and $N_2$, to investigate the effect of dilutions on flame location, shape and heat release rates. The authors concluded that the effect of $N_2$ was negligible, while the effect of $CO_2$ dilution on flame location was measurable. Ćosić [21] used a CCD camera with an optical filter to investigate a correlation between $CH^*$ and air coefficient in a laminar premixed $C_3H_8$ flame of an atmospheric burner with controlled flow rates of air and fuel. The linear correlation between $CH^*$ and air coefficient was found. Ballachey and Johnson [22] investigated blow-off conditions of a low swirl burner using particle image velocimetry (PIV) for different compositions of fuel ($CH_4$, $H_2$, $CO_2$, and CO), different burner geometries and swirl number. Littlejohn and Cheng [23] conducted experimental investigation of different fuel compositions ($CH_4$, $C_2H_4$, $C_3H_8$, $H_2$, $CO_2$, and $N_2$) on lean blow-off velocity in a gas turbine low swirl injector, using PIV. The authors concluded that the swirl injector operated well without need for significant changes, but further studies were needed when burning mixtures with $H_2$. Khallil and Gupta [24] investigated turbulent, confined, swirling combustion, using premixed and non-premixed $CH_4$-air mixture with the air-to-fuel equivalence ratio from 1.25 to 2.0, at constant heat load. The flame $OH^*$ chemiluminescence was captured using an ICCD camera fitted with a 307 nm optical filter. The $NO_x$ and CO emissions were

measured and analyzed. The images of $OH^*$ showed the increased distributed combustion when an extended flue gas exit tube inside the combustor was present, leading to a higher residence time, improved CO emission at low levels of $NO_x$ emission.

Regarding premixed, lean, turbulent, swirl, confined combustion of biogas, using $CH^*$ chemiluminescence imaging technique, there are a few published papers in the available literature. Shi *et al.* [25] used tubular confined flame, $CH_4$ fueled burner with tangential injection of pure $CH_4$, or $CH_4$-$CO_2$ mixtures, and through separate ports, pure oxygen, or oxygen-$CO_2$ mixture. The conventional digital cameras for flame imaging were used, while the $OH^*$, $CH^*$ chemiluminescence images were acquired by a high speed intensified video camera and optical filters. The authors found that the direct images were unclear to understand while $CH^*$ chemiluminescence images enabled understanding of the flame position, structure and behavior. No Abel deconvolution was applied, despite the flame was axisymmetric. Instead, the images were taken from the flame-sidewise and flame-top positions. The CHEMKIN-Pro software was used to calculate the chemical reaction times and laminar burning velocities. The authors analyzed flame images, flame stability and $CH^*$ radical distribution as a function of oxygen-$CO_2$ dilution and equivalence ratio variables. Lafay *et al*. [26] investigated effects of $CO_2$ on combustion of $CH_4$ and simulated biogas ($CH_4$, $CO_2$, and $N_2$) at different air coefficients, in a swirl, premixed, confined flame burner, using a scientific grade ICCD camera for visualization of $CH^*$ radical. The velocity profiles were provided by a laser Doppler anemometry. The authors investigated flame stability and flame structure. Biogas showed narrower flame stability limits than pure methane. The presence of $CO_2$, for the same values of air coefficient, strongly affected reaction zone location. The authors found that the laminar flame speed was the main parameter for the prediction of flame structure.

The present investigation aims at characterization and analysis of premixed, lean, turbulent, swirling, unconfined flames of $CH_4$ and $C_3H_8$ diluted with $CO_2$, using flame $CH^*$ emission imaging technique by means of a commercial CCD camera fitted with an optical filter. The investigation has shown that under laboratory conditions, the applied $CH^*$ imagine technique can reveal flame geometry and locate the flame front with the precision of the order of millimeters. There have been numerous investigations of lean, premixed, confined swirling flames of biogas, using chemiluminescence spectroscopy, ICCD and CCD cameras. Among them only a few investigations used a commercial CCD camera for the flame $CH^*$ emission imaging, and to our best knowledge, there is a lack of such investigations under flame unconfined conditions in the open literature.

## Experimental facility

The experimental facility consisted of a laboratory scale swirl burner, a fuel and air supply system. Schematics of a swirling flow and the burner are shown in fig. 1. The burner was purposely designed for research of lean, premixed, low $NO_x$ and CO emission, gaseous fuel combustion [27]. The burner can burn low calorific value gases, such as, biogas, landfill and natural gas with increased content of $CO_2$ and $N_2$, with 10:1 thermal power dynamic range, avoiding flame flashback and combustion instabilities.

The fuel and air are injected independently, each through six ports, perpendicular to the burner axis at the entrance section. The length of the annular section, from fuel/air injection ports to the annulus exit is twenty annulus widths. The premixing of fuel and air is performed in the burner annulus. The quality of mixing of fuel and air was checked and found that the differences between actual and perfect premixing were better than ± 5% [27]. A flat-vane, axial flow swirler, with vane angle of $45^o$ is mounted in the annulus, at 20 mm before the burner exit.

The $CH_4$ and $C_3H_8$ were used as basic fuels. Biogas, landfill gas and lower calorific value natural gases were simulated by addition of $CO_2$ into $CH_4$. Fuels and $CO_2$ were supplied from pressurized cylinders, while the air was supplied by a fan. The uncertainty of flow rate measurements for $CH_4$, $C_3H_8$, and $CO_2$ was ±5% (rotameters manufactured by Dwyer Instruments, Inc.), while the air-flow rate uncertainty was ±3% (orifice flow meter; BS 1042 fluid-flow in closed conduits). The quality of $CH_4$ and $C_3H_8$ was 99.5%, while the quality of $CO_2$ was 99.995%. The experiments were performed at constant nominal thermal power of 4 kW, the corresponding Reynolds number was 8500-12000, depending on fuel type and $\lambda$. The $CO_2$ content and air-to-fuel equivalence ratio were systematically and independently varied, as shown in tab. 1.

**Table 1. Fuel composition and air-to-fuel equivalence ratios**

| Fuels | $CO_2$ content in fuel-$CO_2$ mixture, [%] | Air to fuel equivalence ratio, $\lambda$ |
|---|---|---|
| Methane and propane | 0, 10, 20, 30, 40 | 1.0, 1.1, 1.2, 1.3, 1.4 |

## Flame imaging and image processing

A Nikon D80 digital camera with Nikkor AF f 4-5.6D ED 70-300 mm telephoto lens fitted with a narrow band optical filter was used for the $CH^*$ emission imaging of flame. An optical filter was chosen to fit the $CH^*$ chemiluminescence emission which is centered at 430 nm. Technical details of the imaging system are given in tab. 2.

**Table 2. Camera and optical filter details**

| Camera | Nikon D80; DSLR |
|---|---|
| CCD sensor | APS-C 10.8 MP; 23.6 mm × 15.8 mm Nikon DX format |
| Resolution | 3.872 × 2.592 (10.2 effective megapixels) |
| Telephoto lens | Nikkor AF f 4-5.6D ED, zoom 70-300 mm |
| Optical filter | Ealing 35-3300, 430.0 ±2.0 nm, transparency 51% |
| | attenuation of other wave lengths >99% |

Preliminary investigation and analysis were taken to set the CCD sensor sensitivity, camera exposure time and aperture, keeping in mind that the entire flame should be in focus, which is controlled by the camera aperture setting. The lower CCD sensor sensitivity produces lower noise in images while longer camera exposure improves signal to noise ratio. The final settings of the CCD sensor sensitivity, camera exposure time and aperture were ISO 200, 3 seconds and f8, respectively [28].

The preliminary investigation showed that the exposure time of 2 ms was fast enough to get the images that revealed turbulence-flame structures, as can be seen in fig. 2(a). The exposure time of 3 seconds produced images without noticeable turbulence-flame structures fig. 2(b).

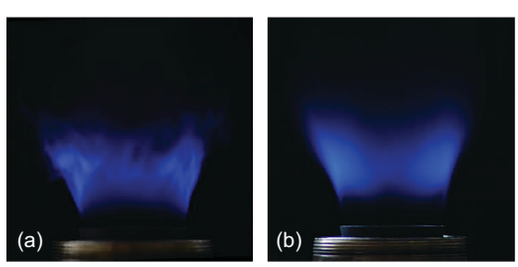


**Figure 2. Flame images taken without optical filter; exposure time 2 ms (a) and 3 seconds (b).**

In order to get images which $CH^*$ emission intensities can be compared, the highest value of the acquired light intensity of the investigated flames, was set 250 on the grey scale level of 0-255. In practice this corresponded to the $C_3H_8$-air stoichiometric flame. Consequently, the maxima of the acquired $CH^*$ emission intensities for all other cases: $C_3H_8/CO_2$,

$CH_4/CO_2$ mixtures, and $\lambda > 1.0$, were less than 250. The effective format of images was 249 pixels per line ($x$-co-ordinate) and 204 pixels per field ($z$-co-ordinate).

The acquired luminescence images of flames were processed by in house developed software [21]. To get an impression of the $CH^*$ intensity distribution on the 0-255 scale, is shown in fig. 3.

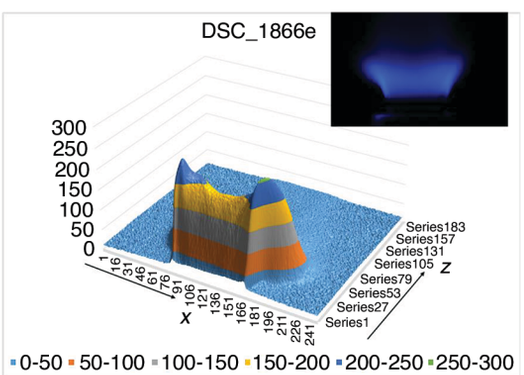


**Figure 3. Illustration of acquired CH* chemiluminescence; the values are given in arbitrary units (*a.u.*); $C_3H_8$-air flame, $\lambda$ = 1.0, $CO_2$ = 0%**

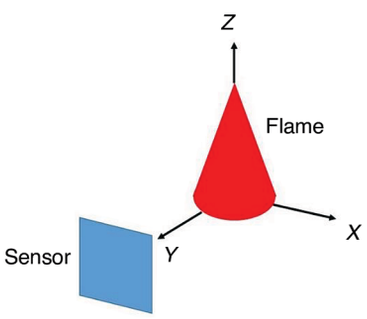


**Figure 4. The Abel transform co-ordinate system.**

The Abel deconvolution was done numerically using in-house developed software to be published in 2019. The flame was considered axisymmetric with a local $CH^*$ luminescence intensity $i = i(x, y, z)$, as a function of the radial distance $r$, $r^2 = x^2 + y^2$, and the co-ordinate $z$, fig. 4. One should note that the beginning of the co-ordinate $x$ differs in the two co-ordinate systems, as shown in figs. 3 and 4.

The flames are assumed axisymmetric, therefore, one half of an image represents the flame as a whole. In the first step of the image analysis, the image zone with the highest values of grey level of CH* emission intensity is assumed the flame zone [7, 8]. In the next step, the Abel deconvolution is applied to find the grey level distribution in the flame zone.

## Results and discussion

The photographs of $CH^*$ emission intensity are used for the qualitative and quantitative interpretation of flame geometry and location. The flame location is assumed a zone with the local maxima of $CH^*$ emission intensity [7]. As most of the original photographs were too dim for a naked eye, they are shown here in their inverted forms.

It is important to stress that the combustion took place under unconfined conditions which affects the flame due to the entrainment of the cold ambient air into the flame zone which increases the local content of air in the fuel-air mixture, decreases the flame temperature and increases the required time for chemical reactions. As a consequence, the flame location is shifted downstream. Besides, the flame may become prone to instabilities and flame blow-off can occur, as well. The increased mean velocity of the injected mixture of fuel and air, with the increase of nominal $\lambda$, further adds to the air entrainment effects due to the increased fuel-air flow momentum and turbulence intensity. Geometry, dimensions and location of flame depend on burner geometry, swirl number, Reynolds number, turbulence, fuel type, air-to-fuel equivalence ratio, laminar and turbulent flame speeds, confinement and other parameters [4, 11-13]. A swirl induces recirculating annular vortex, entrains fresh air, as mentioned before, but also re-circulates the combustion products with the incoming fresh fuel-air mixture, thus increasing the stability of

flame. The re-circulating flow, produced by the swirl and the center bluff-body, stabilizes the flame in an annular vortex flow. In addition, the expansion of high temperature combustion products tends to shift the flame in outward direction further adding to flame geometry.

The acquired $CH^*$ emission images of $C_3H_8$ flames, as a function of $\lambda$ and $CO_2$, are shown in fig. 5. The intensity of $CH^*$ emission is presented in the arbitrary units (a.u.). When the air-to-fuel equivalence ratio increases from 1.0 to 1.4, the mean exit velocity of $C_3H_8$-air mixture increases 1.4 times, the adiabatic flame temperature decreases from 2257 to 1920 K and the laminar flame speed decreases from 0.41 to 0.26 m/s [13]. The flame becomes narrow and shifted downstream, as can be seen in figs. 5(a)-5(b), and 5(c)-5(d). The effect of $CO_2$ dilution, for $\lambda$ = constant, is shown in figs. 5(a)-5(c) and 5(b)-5(d). As can be seen, the effect of $CO_2$ on flame geometry and location is small because even the maximum $CO_2$ = 40% dilution increases the mean velocity of fuel-$CO_2$-air mixture less than 2%, while the stoichiometric, adiabatic flame temperature decreases from 2257 to 2211 K, or 2.0% [13], resulting in the flame which is marginally shifted downstream.

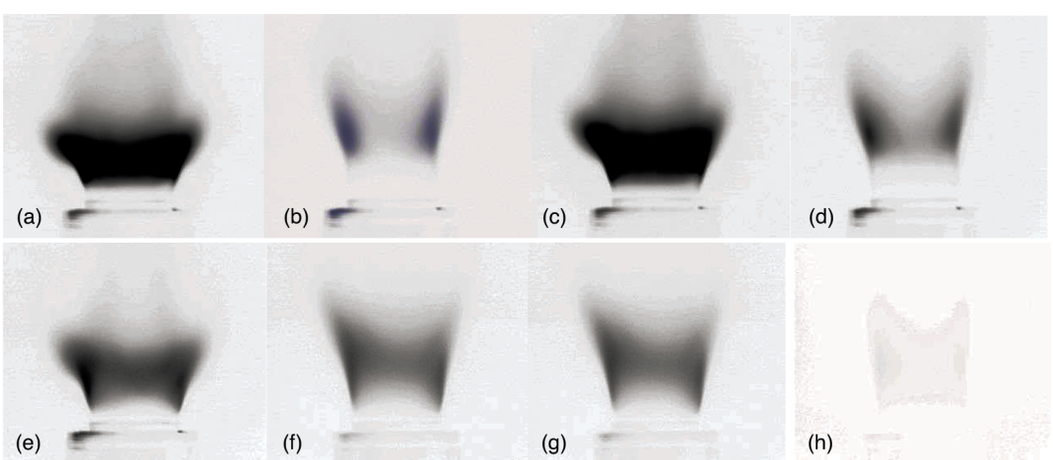


**Figure 5. Effect of $CO_2$ and $\lambda$ on $CH^*$ emission of $C_3H_8$ (1st row) and $CH_4$ (2nd row) flames; (a), (e) $\lambda$ = 1.0, $CO_2$% = 0; (b), (f) $\lambda$ = 1.4, $Co_2$% = 0; (c), (g) $\lambda$ = 1.0, $CO_2$% = 40; (d), (h) $\lambda$ = 1.4, $CO_2$ = 40%**

In order to illustrate the flame shapes and locations in a visually more comparable way, the halves of images are presented together, as shown in fig. 6.

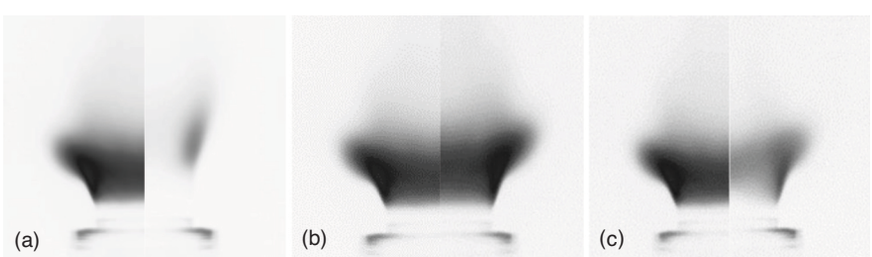


**Figure 6. (a) Effect of $\lambda$ on $CH^*$ emission of $C_3H_8$ flame; $CO_2$ = 0%, $\lambda$ = 1.0 (left half of image) and $\lambda$ = 1.4 (right half); (b) effect of $CO_2$ on $CH^*$ emission of $C_3H_8$ and $C_3H_8$-$CO_2$ flame, $\lambda$ = 1.0, $CO_2$ = 0% (left half) and $CO_2$ = 40% (right half); (c) effect of fuel type on $CH^*$ emission, $\lambda$ = 1.0 and $CO_2$ = 0%, $C_3H_8$-air (left half) and $Ch_4$-air flames (right half)**

The $CH^*$ emission of $C_3H_8$ is about two times greater than that of $CH_4$ due to the favorable molecule structure of $C_3H_8$, regarding the production of $C_2H$, the key radical for $CH^*$ chemiluminescence emission.

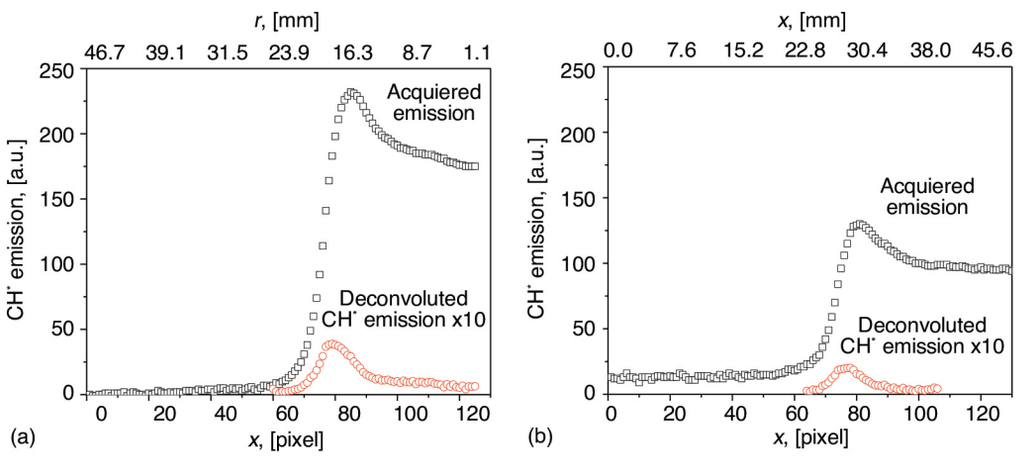


**Figure 7. The $CH^*$ emission and Abel deconvoluted curves; $C_3H_8$ (a), $CH_4$ (b); $\lambda$ = 1.0, $CO_2$ = 0%**

Concerning the $CH^*$ emission intensity a typical example is shown in fig. 7. One should note that in order to make the curves visually comparable, the true values of the Abel deconvoluted curves are multiplied by 10. The deconvoluted $CH^*$ curve peak area, fig. 7, represents a flame zone where the main chemical reactions take place. It is worth noting that the location of the flame zone is between the inflection point and the peak of the $CH^*$ emission curves.

The effects of fuel type, air-to-fuel equivalence ratio and $CO_2$ content on $CH^*$ emission are compared and analyzed. The deconvoluted $CH^*$ emissions of $CH_4$ and $C_3H_8$ in the radial direction, as a function of $CO_2$ content and $r$, are presented in fig. 8. The results show that the $CH^*$ emission intensity of $C_3H_8$ flame is about twice the intensity of $CH_4$ flame. This is because the main reaction path for $CH^*$ emission is via $C_2H$ radical, the main $CH^*$ precursor, which concentration is higher in $C_3H_8$ than in $CH_4$ flames. The flame zone of $CH_4$ is narrower compared to the $C_3H_8$ flame zone. The effect of $CO_2$ dilution is small; the intensity maxima are marginally

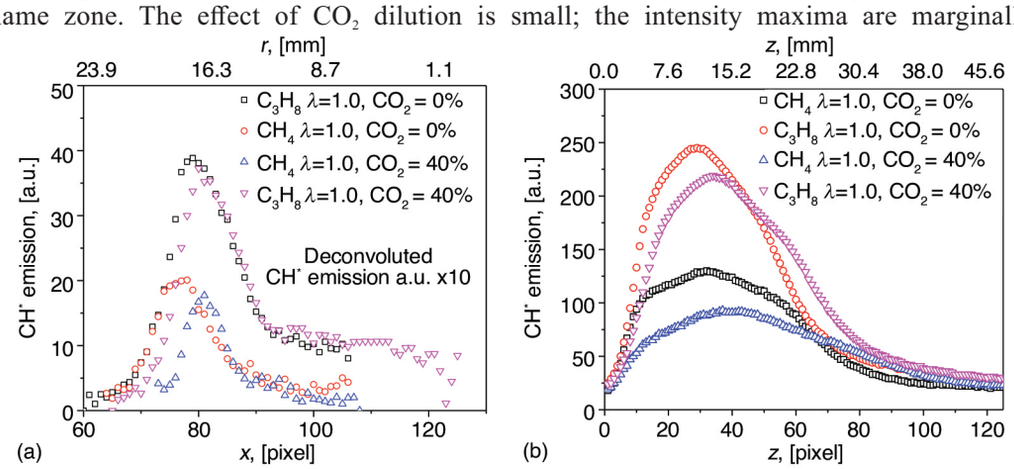


**Figure 8. The $CH^*$ distribution in radial direction (a) and in axial direction (b), as a function of fuel type and $CO_2$ content, at stoichiometric conditions.**

lower and slightly shifted, about 1 mm, towards the axis. This is expected as the $CO_2$ dilution slightly decreases the adiabatic flame temperature.

The $CH^*$ emission peaks for all flames in the radial direction, as presented in figs. 8, are located in the 2 mm thick zone, with marginal shift of the $CO_2$ diluted flames towards the flame axis. The presence of $CO_2$ shifts $CH^*$ peaks about 3 mm downstream. It is interesting to note that the peaks of $CH^*$ emission can be located with the precision of order of millimeters.

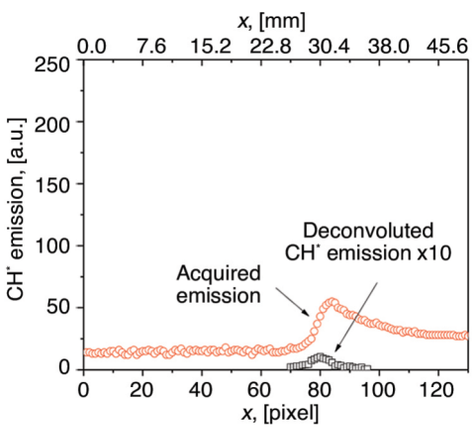


**Figure 9. The $CH^*$ emission radial distribution of $CH_4$ flame: $\lambda$ =1.4, $CO_2$ = 0%**

As already mentioned and again confirmed in fig. 8 the $CH^*$ emission intensity is greater for $C_3H_8$ *vs.* $CH_4$ flames due to chemical structure of $C_3H_8$, which favors production of $C_2H$, the main precursor of $CH^*$. The increase of $\lambda$ from 1.0 to 1.4 decreases the $CH^*$ emission to about one half of its value for $\lambda = 1.0$. The radial distribution of $CH^*$ emission of lean $CH_4$-air flame is shown in fig. 9.

The effect of $\lambda$ on flame location in axial direction is pronounced, on the contrary to the effect of $CO_2$, which is small, as can be seen in fig. 10.

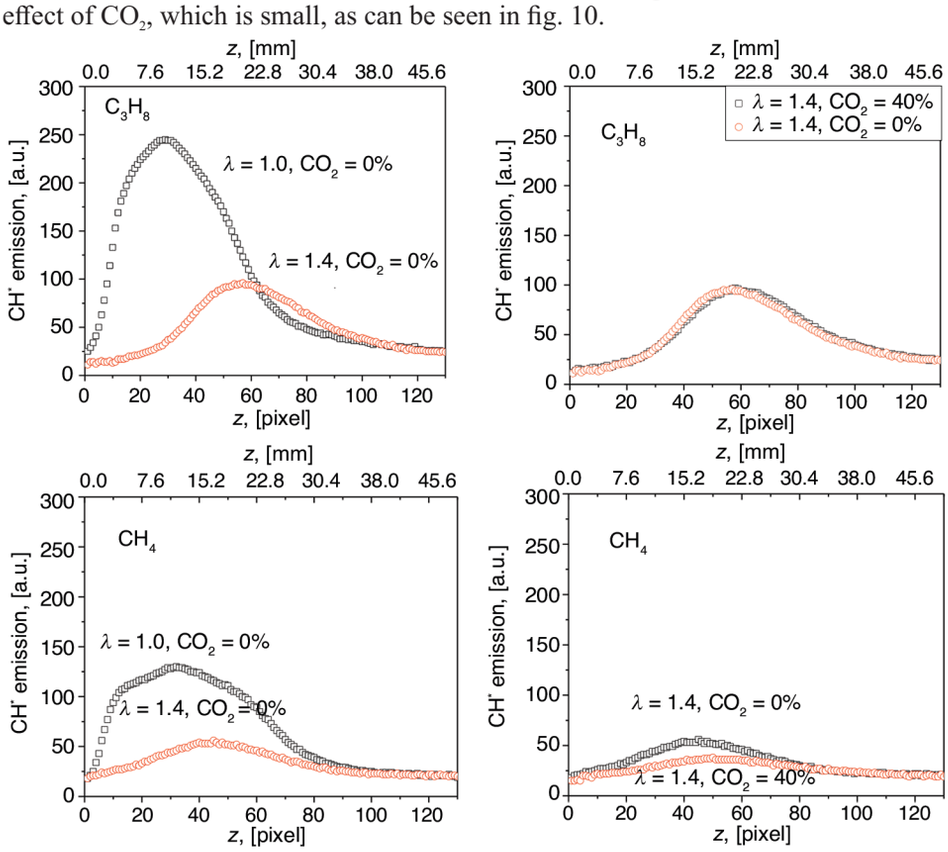


**Figure 10. The $CH^*$ axial distribution of $C_3H_8$ and $CH_4$ flames as a function of $\lambda$ and $CO_2$.**

In conclusion, regarding the present investigation, there have been numerous, published investigations based on flame chemiluminescence, but rather limited number on biogas and hydrocarbon gases diluted with $CO_2$. Mostly, chemiluminescence emission has been acquired and measured using specialized spectroscopic equipment, but quite small number using a commercial CCD camera. When it comes to the premixed, turbulent swirling flames of biogas or $CH_4$ diluted with $CO_2$, the number of published papers is very limited. Shi *et al*. [25] and Lafay *et al*. [26] performed investigations similar with the present one, but with very important differences. The authors [25] investigated confined, not premixed flame of $CH_4$ and pure $O_2$, or $O_2$ and $CO_2$ mixtures without Abel deconvolution. Instead they took the images in line with the combustor axis, at upstream and downstream positions. Investigation of Lafay *et al*. [26] can be considered most similar with the present one, but also with important differences. The authors used a simulated biogas to analyze the velocity field, flame structure, flame speed and the instability frequencies, but under the confined flame conditions. They found that the flame structure was directly linked to the laminar flame speed with the bifurcated flame, located in the corner and in the internal (close to the combustor axis) re-circulation zones.

## Conclusion

The effects of fuel type, the $CO_2$ dilution (simulated biogas) and air-to-fuel equivalence ratio on the flame geometry and location, for the swirling, lean, premixed flame under unconfined conditions, have been investigated, using a commercial CCD camera and a $CH^*$ chemiluminescence imaging technique. The $C_3H_8$ *vs*. $CH_4$ showed about two times stronger $CH^*$ emission intensity. Air to fuel equivalence ratio had strong effect on the flame shape and location, while the effect of $CO_2$ was of minor importance. Both, $CH_4$ and $C_3H_8$ were similarly affected with the presence of $CO_2$. There was strong effect of air to fuel equivalence ratio on the $CH^*$ intensity, flame geometry and location. The increase of air-to-fuel equivalence ratio decreased the $CH^*$ intensity, made the flame mostly narrower and shifted downstream. For the stoichiometric mixtures of both fuels, the $CO_2$ decreased the $CH^*$ emission intensity to some extent and slightly shifted the flame downstream. For lean mixtures of both fuels ($\lambda$ = 1.4) the effect of even the highest concentration, $CO_2$ = 40%, was practically insignificant. The flames were slightly narrower and shifted marginally downstream. The results showed, that using a commercial CCD camera, fitted with an optical filter, the $CH^*$ chemiluminescence imaging technique was suitable method for the flame geometry and location analysis of the turbulent, swirling, premixed, unconfined flame of $C_3H_8$ and $CH_4$, diluted with $CO_2$.

## Acknowledgment

The authors would like to thank the Editorial Board for the invitation to submit a paper to this special issue of the Thermal Science International Scientific Journal dedicated to honor Professor Milan Radovanović on the occasion of his 80th birthday.

## References

[1] ***,The European Commission, The Paris Agreement 2015, https,//ec.europa.eu/clima/policies /international/negotiations/paris_en
[2] Chomiak, J., *et al*., Combustion of Low Calorific Value Gases, Problems and Prospects, *Progress in Energy and Combustion Science*, *16* (1989), 2, pp. 109-129
[3] Kexin, L., Sanderson, S., The Influence of Changes in Fuel Calorific Value to Combustion Performance for Siemens SGT-300 Dry Low Emission Combustion System, *Fuel, 103* (2013), Jan., pp. 239-246
[4] Ballachey, G. E., Johnson, M. R., Prediction of Blow Off in a Fully Controllable Low-Swirl Burner Burning Alternative Fuels: Effects of Burner Geometry, Swirl, and Fuel Composition, *Proceedings of the Combustion Institute, 34* (2013), 2, pp. 3193-3201

[5] Jensen, J., B., Luminescence Techniques Instrumentation and Methods, *Radiation Measurements*, *27* (1997), 5-6, pp. 749-768
[6] Bheemul, H., *et al*, Three-Dimensional Visualization and Quantitative Characterization of Gaseous Flames, *Meas. Sci. Technol. 13* (2002), 10, pp. 1643-1690
[7] Hardalupas, Y., Orain, M., Local Measurements of the Time-Dependent Heat Release Rate and Equivalence Ratio Using Chemiluminescence Emission from a Flame, *Combustion and Flame, 139* (2004), 3, pp.188-207
[8] Guethe, F., *et al*., Chemiluminescence as Diagnostic Tool in the Development of Gas Turbines, *Appl Phys B*, *107* (2012), 3, pp. 619-636
[9] Orain, M., Hardalupas, Y., Effect of Fuel Type on Equivalence Ratio Measurements Using Chemiluminescence in Premixed Flames, *Comptes Rendus Mecanique, 338* (2010), 5, pp. 241-254
[10] Markandey, T., *et al*., Chemiluminescence-Based Multivariate Sensing of Local Equivalence Ratios in Premixed Atmospheric Methane-Air Flames, *Fuel*, *93* (2012), Mar., pp. 684-691
[11] Syred, N., Beer, J. M., Combustion in Swirling Flows - A Review, *Combustion and Flame,23* (1974), *2*, pp. 143-201
[12] Gupta. A., *et al*., *Swirl Flows*, Abacus Press, Preston, UK, 1984
[13] Lefebvre, A. H., *Gas Turbine Combustion*, Taylor & Francis, Philadelphia, Penn., USA, 1998
[14] Merzkirch, W., *Flow Visualization*, Academic Press, New York, USA, 1974
[15] Post, H., F., Walsum, T., Fluid Flow Visualization, in: *Focus on Scientific Visualization*, (Eds., Hagen, H., Muller, H., Nielson, G.,) Springer Verlag, Berlin, 1993, pp. 1- 40
[16] Gaydon, A., Wofhard, H., *Flames, Their Structure, Radiation and Temperature*, Chapman and Hall, London 1960
[17] Simona, S., *et al.*, Chemiluminescence Analysis of the Effect of Butanol-Diesel Fuel Blends on the Spray Combustion Process in an Experimental Common Rail Diesel Engine, *Thermal Science*, *19* (2015), 6, pp. 1943-1957
[18] Jozsa, V., Sztanko, K., Flame Emission Spectroscopy Measurement of a Steam Blast and Air Blast Burner, *Thermal Science*, *21* (2017), 2, pp. 1021-1030
[19] Guiberti, T., *et al*., Flame Chemiluminescence from $CO_2$ - and $N_2$-Diluted Laminar $CH_4$/Air Premixed Flames. *Combustion and Flame*, *181*, (2017), pp. 110-122
[20] Marsh, R., *et al*., Premixed Methane Oxy-Combustion in Nitrogen and Carbon Dioxide Atmospheres, Measurement of Operating Limits, Flame Location and Emissions. *Proceedings of the Combustion Institute*, *36* (2017), 3, pp. 3949-3958
[21] Ćasić, B., Experimental Photometric Research of Laminar Premixed Flame, (in Serbian), Ph. D. thesis, Faculty of Mechanical Engineering, University of Belgrade, Belgrade, 2013
[22] Ballachey, G., Johnson, M., Prediction of Blow off in a Fully Controllable Low Swirl Burning Alternative Fuels - Effects of Burner Geometry, Swirl, and Fuel Composition, *Proceedings of the Combustion Institute*, *34*, (2013), 2, pp. 3193-3201
[23] Littlejohn. D., Cheng, R., K., Fuel Effects on a Low Swirl Injector for Lean Premixed Gas Turbines, *Proceedings of the Combustion Institute*, *31* (2007), 2, pp. 3155-3162
[24] Khallil, A., Gupta, A., Swirling Distributed Combustion Foe Clean Conversion in Gas Turbine Applications, *Applied Energy, 88* (2011), 11, pp 3685-3693
[25] Shi, B., *et al*., Carbon Dioxide Diluted Methane/Oxygen Combustion in a Rapidly Mixed Tubular Flame Burner, *Combustion and Flame, 162* (2015), 2, pp. 420-430
[26] Lafay, Y., *et al*., Experimental Study of Biogas Combustion Using a Gas Turbine Configuration, *Proceedings*, 13th, Symposium on Laser Techniques to Fluid Mechanics, Lisbon, 2006
[27] Adzic, M., *et al.*, Effect of a Microturbine Combustor Type on Emissions at Lean-Premixed Conditions. *Journal of Propulsion and Power*, 26 (2010), 5, pp. 1135-1143
[28] Adzic, M., *et al*., Error Analysis and Calibration Procedure When Using an ICCD Camera for the Study of Spray Formation, *Journal of Flow Visualization and Image Processing*, *4* (1997), 2, pp. 149-162

Paper submitted: March 12, 2018
Paper revised: September 3, 2019
Paper accepted: September 26, 2019